Indonesian Journal of Science & Technology

Journal homepage: http://ejournal.upi.edu/index.php/ijost/

Investigation of a Cruising Fixed Wing Mini Unmanned Aerial Vehicle Performance Optimization

Shahrooz Eftekhari, Abdulkareem Sh. Mahdi Al-Obaidi

Taylor's University Lakeside Campus No. 1, Jalan Taylors, 47500 Petaling Jaya, Selangor, Malaysia

Correspondence: E-mail: abdulkareem.mahdi@taylors.edu.my

A B S T R A C T

The applications of unmanned aerial vehicles have been extended through the recent decades and they are utilized for both civil and military applications. The urge to utilize unmanned aerial vehicles for civil purposes has elevated researchers and industries interest towards the mini unmanned aerial vehicle (MUAV) category due to its suitable configurations and capabilities for multidisciplinary civil purposes. This study is an effort to further enhance the aerodynamic efficiency of MUAVs through a parametric study of the wing and proposing an innovative bioinspired wing design. The research is conducted utilizing numerical simulation and experimental validation. This research provides a better understanding of different wing parameter(s) effect on the aerodynamic performance of the wing and mini unmanned aerial vehicles. A new wing configuration is designed, implemented and evaluated. The wing is named as Alpine since it is inspired by biomimicry of alpine swift bird. Evaluation of the new wing geometry shows that the Alpine wing geometry performs 35.9% more efficient compared to an existing wing with similar wing area. Hence, the aerodynamic efficiency optimization is achieved for the Alpine wing which helps to enhance the performance of MUAVs.

1. INTRODUCTION

The application of unmanned aerial vehicles (UAVs) has been extended recently and they are not only utilized for military purposes, but also are widely applied for civil purposes in agriculture, search and rescue, powerline inspection, etc. (Chahl, 2015). Thus, researchers and industries attention are brought towards the Mini-UAV (MUAV) class of UAVs due to its suitable configuration and capabilities for multidisciplinary purposes (Shukla and Karki, 2016). The MUAVs fly at low speed and small length scale which put them in low wing chord Reynold number flight regime ranging from $1.5×10^4$ to $5×10^5$ (Ghazzai *et al.*, 2017). The aerodynamic performance of MUAVs is critically dependent on their lifting surface which is the wing and its airfoil section.

It is observed in the literature, several MUAVs have been designed and implemented; however, there is still room for developing new solutions and designs to optimize their performance. Aerodynamic efficiency is one of the effective tools to enhance the performance of MUAVs (Kontogiannis and Ekaterinaris, 2013). The aerodynamic efficiency optimization can be compromised through the modification of wing configuration and its parameters such as airfoil, aspect ratio, tapper ratio, sweep as well as the wing shape (Abdulrahim *et al.*, 2010; Bronz *et al.*, 2013; Panagiotou *et al.*, 2014). The laminar boundary flowing over an airfoil at low speed flight regime separates near the leading edge of the airfoil resulting in generation of laminar separation bubbles occupying 10% to 40% of the airfoil surface at low Reynold numbers. Literature studies show the need to utilize efficient low speed airfoil designs for MUAVs since they fly at chord Reynolds numbers less than $5×10^5$ (Ananda *et al.,* 2015; Hain *et al.*, 2009; Mueller *et al.*, 2003).

The aerodynamic performance of wings with different aspect ratios were investigated at Reynolds number range of 10^4 to 10^5 and

it is observed that increasing the aspect ratio significantly helps in reduction of the drag coefficient by reducing the effect of wing tip vortex on the flow around the wing. Also, it is observed that the aerodynamic performance of wings at very low Reynolds number regime below $5×10^4$ has a significantly different pattern compared to cases with higher Reynolds numbers. Observations indicate that at very low Reynolds number flight regime and low angles of attack where the free stream velocity is very low, the drag coefficient is reduced as the Reynolds number is increased. Such phenomena are observed at very low speed flight regime due to the delay in laminar separation of the flow from the wing surface. The similar behavior is also observed on other airfoils tested at very low Reynolds numbers (Kim and Chang, 2014; Martínez-Aranda *et al.*, 2016).

Another suggested method to improve the aerodynamic efficiency of low speed wings is to reduce the span wise lift coefficient towards the wing tip by reducing the tapper ratio and utilizing trailing notches on wings (Drovetski, 1996; Sathaye *et al.*, 2004; Selig *et al.*, 1998). The effect of wing tip vortices is observed to be significantly reduced on wings with such design. Thus, the span wise lift coefficient peaked value at wing tip area is significantly reduced which helps to enhance the aerodynamic efficiency of the wing at low Reynold numbers (Eftikharia and Al-Obaidi, 2019; Kumar *et al.*, 2017).

Research continues to develop more reliable and feasible MUAVs to be utilized in different applications. This research is an effort to further enhance the aerodynamic efficiency of MUAVs through parametric study of the wing and proposing a new wing design. The research provides a better understanding of the influence of different wing parameters such as airfoil shape, tapper ratio ($λ$), aspect ratio (AR), and span (b) on the aerodynamic performance of MUAVs. A new wing configuration with enhanced aerodynamic efficiency and increased flight endurance is designed and implemented to

benefit industries such as aviation, agriculture, health care as well as oil and gas.

2. METHODOLOGY

The parameters which have significant effect on the aerodynamic efficiency of MUAVs are initially identified through numerical simulations and used in design of a new wing configuration. The wing aerodynamic characteristics are numerically predicted and validated using wind tunnel experiments for selected wing models with optimized aerodynamic efficiency. The experiments are conducted utilizing Taylor's University wind tunnel (TUWT) which is an open subsonic wind tunnel with 0.3 × 0.3 m and a length of 0.8 m test section . The aerodynamic forces are measured using the TUWT force measurement system equipped with an ATI GAMMA 6 axis F/T transducer.

Test models with wing parameters shown in **Table 1** are compared to identify the contribution of the parameter changes to aerodynamic efficiency of the wing configurations. To have a valid comparison for different wing configurations, the wing frontal area is set to 0.0225 m^2 for all the wings investigated in this research. The selected value for wing area is calculated based on the maximum allowable blockage in TUWT test section. The wing span (b), root chord (C_r) and tip chord (C_t) are calculated and adjusted based on the investigated aspect ratio (AR) and frontal area (A) using

Eq. (1), for rectangular wings ($C_t = C_r$) using Eq. (2) and trapezoidal wings ($C_t = 0.5 \times C_r$) using Eq. (3).

$$b = \sqrt{AR \times A} \tag{1}$$

$$C_r = \frac{A}{b} \tag{2}$$

$$C_r = \frac{4 \times A}{3 \times b} \tag{3}$$

The aerodynamic efficiency (c_l / c_d) of seven well known low speed airfoils are compared and the most efficient airfoil is selected for the wing designs and numerical simulations are conducted on the wing configurations using ANSYS FLUENT. The aerodynamic efficiency of the airfoils are available in the "Summary of Low-Speed Airfoil Data" (Giguere and Selig, 1998). Once the most efficient airfoil is selected, the wing models are designed based on the calculated dimensions and research enters the numerical simulation phase. The chord Reynolds number (Re$_c$) is maintained at 2×10^5 throughout the investigation to achieve the physical similarity with the reference published data. The length of the mean aerodynamic chord used in Re calculation is equal to the root chord for rectangular wings while for non-rectangular it is calculated using Eq. (4).

$$\overline{C} = \frac{2 \times [C_r^2 + (C_r \times C_t) + C_t^2]}{3 \times (C_r + C_t)} \tag{4}$$

Table 1. Investigation of wing parameters.

	Case 1	Case 2	Case 3	Case 4	Case 5
AR	1	1	1	1.8	1.8
λ	1	0.5	0.5	0.5	0.5
Sweep C/4 Angle	0	16	0	16	0

2.1 Computational Method

2.1.1. Computational domain, solver and turbulence model setup

The flow is incompressible since the Mach number is less than 0.3. Hence, a pressure-based solver is selected, and the properties of the fluid are presented in **Table 2.** The simulations on all the wing geometries are conducted at Re 2×10^5 and 0° degrees angle of attack which is the corresponding angle of attack at cruise condition.

The fluid domain is generated using a C-type grid since it is observed to be the reliable grid type for low speed airfoil geometries based on literature investigations (Shah *et al.,* 2015). The fluid domain boundaries are set to have a distance of 20 chords away from the wing geometry to allow the flow to be well developed before and after the wing geometry (**Figures 1 and 2**). The Spalart - Allmaras turbulence model is selected for the simulations as it was investigated by

Lei (2005) and it is found to be the efficient and applicable turbulent model for wing simulations at low speed.

2.1.2. Mesh independency

The efficiency of fluid domain mesh around the wing geometry is crucial for accurate prediction of the aerodynamic efficiency of the wing geometries with minimum convergence time. Several mesh cases with different number of elements, element sizes, sweep and inflation layers are generated to identify the efficient mesh (see **Table 3**). Comparison of different mesh configurations with Selig *et al.* (1998) experimental data shows that a fine mesh with sufficiently thin first layer near the wing and refined near-wall grid resolution (see **Figures 3 and 4**) helps to reduce the wall Y+ value . This allows the Spalart -Allmaras turbulence model to capture more details within the viscous sublayer and the simulation results converge more accurate.
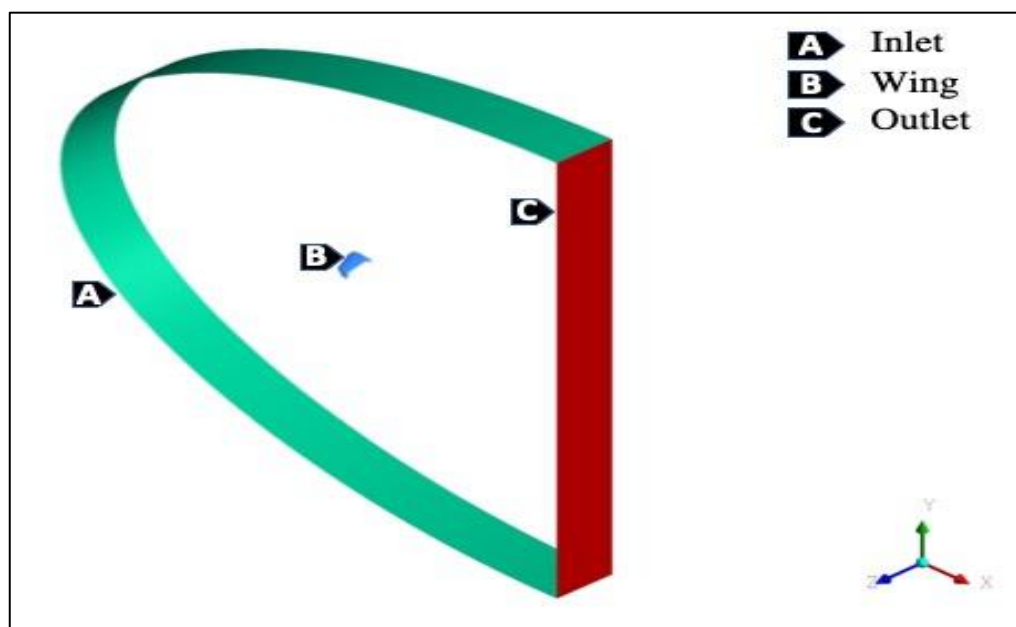

Figure 1. Fluid domain around the wing models.

Table 2. Fluid properties.

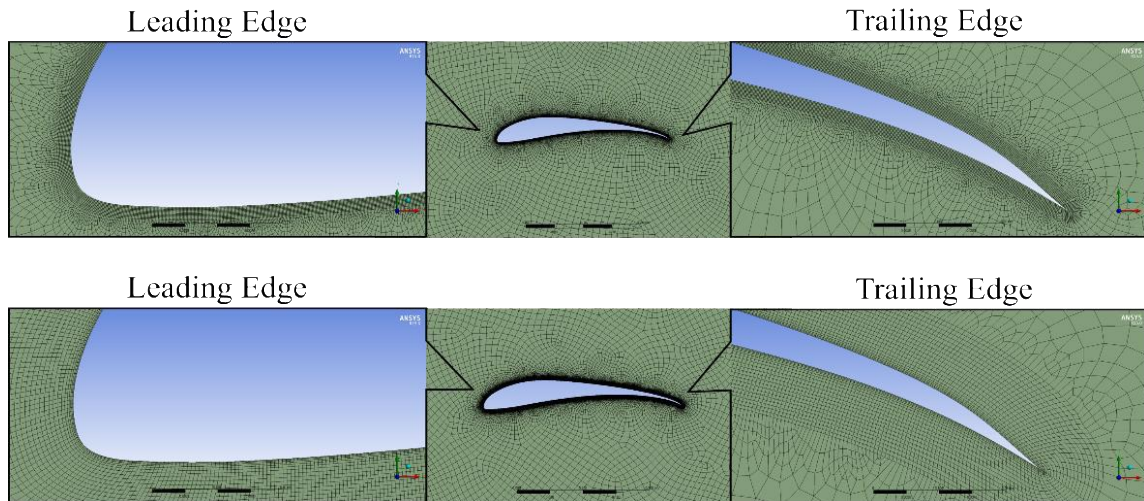| Fluid	Temperature, °	Density, Kg/m³	Viscosity, Kg/m.s
Air	20	1.225	1.789×10^5

Figure 2. Mesh around "Case 2"(top), mesh around "Case 4"(bottom).

Table 3. Mesh efficiency analysis of rectangular wings.

		Case 1	Case 2	Case 3	Case 4	Case 5
	Number of Elements	1.17×10^6	2.81×10^6	1.75×10^6	1.85×10^6	2.12×10^6
	Element Size (m)	5×10^{-5}	1×10^{-4}	1×10^{-4}	1×10^{-4}	8×10^{-4}
C_L	CFD	0.571	0.460	0.403	0.399	0.395
	Difference from Selig Data (%)	60	29	13	11	11
C_D	CFD	0.2408	0.1500	0.0869	0.0868	0.0861
	Difference from Selig Data (%)	205	90	10	10	8
	Simulation Completion Time (Hours)	20	50	70	75	100

The wall Y+ value plays an important role in determination of the accuracy of simulation results. The effect of wall Y+ on the results accuracy in comparison with experimental data of Selig *et al.* (1998) is illustrated in **Figure 3**. The figure shows that the aerodynamic efficiency obtained from simulation differs by 2% for "Case 5" where the wall Y+ is below 5. As the Y+ value is increased to 6 and 9, the percentage error is increased to 3 and 5% in "Case 4" and "Case 3" respectively . However , the simulation solution convergence using "Case 4" mesh is 25 % faster compared to "Case 5" mesh while the accuracy of the aerodynamic efficiency obtained from simulation is not significantly affected . Therefore , "Case 4" mesh is identified as the most efficient mesh and the same method is utilized throughout research.
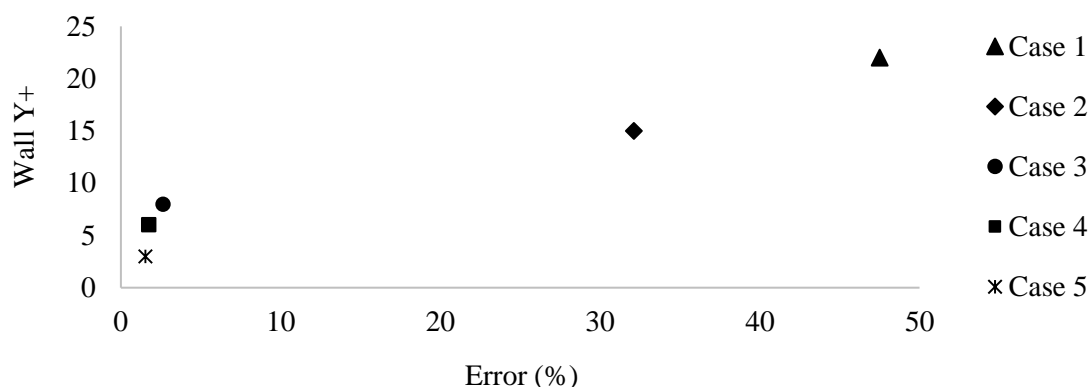
Figure 3. Accuracy of aerodynamic efficiency at different wall Y+.

Figure 4. TUWT (left) and test model installation method (right).

2.2 Wind Tunnel Experiments

The results obtained through simulations on the new wing design are validated by experimental results. The new wing geometries are manufactured using Taylor's University 3-D printing machine and the precision of the manufactured wing geometries is evaluated by comparing the model with printed technical drawing of the wing model prepared using Solidworks 15. The wing models are installed in the TUWT test section through the aerodynamic centre of the test models and the angle of attack is set to 0° (**Figure 4**). The aerodynamic centre (AC) of the wing is calculated using Eq. (5).

$$AC = C/4 \qquad (5)$$

The lift (*L*) and drag (*D*) forces are obtained from the load cell through the experiment. The corresponding coefficients for lift (C_L), drag (C_D) and induced drag (C_{Di}) coefficients are calculated using Eqs. (6), (7), and (8) at the same operating condition mentioned in **Table 1** where the flow measured density (ρ) is 1.225 kg/m^3 and speed (*v)* is adjusted based on MAC of the wing models.

$$L=\tfrac{1}{2}\rho v^2 A C_L \qquad (6)$$

$$D=\tfrac{1}{2}\rho v^2 A C_D \qquad (7)$$

$$C_{Di} = \frac{C_L{}^2}{\pi e AR} \qquad (8)$$

3. RESULTS AND DISCUSSION

3.1 Aerodynamic efficiency of the wings

The performance enhancement of a cruising MUAV has significant impact on power consumption reduction of the aircraft and endurance increment (Kontogiannis and

Ekaterinaris, 2013). One of the common methods to enhance the performance is to optimize the aerodynamic efficiency of the wing configuration.

3.2. Effect of Airfoil Section

The lift force is generated by the airfoil section of wing. It is crucial to carefully select the airfoil(s) that generate the desired pressure distribution around the wing geometry to create maximum lift and minimum drag at given operating conditions. The operating condition of interest in this research is the cruise phase of a MUAV at low subsonic speed where the cruising Reynolds number is in range of 10^5. In such low operating Re, the aerodynamic efficiency and lift coefficient of the airfoil in cruising condition, which is typically at significantly low angles of attack, plays an important role in aerodynamic performance of low speed aircrafts. The investigation of aerodynamic characteristics of different low speed airfoils at low angle of attack is presented in **Figure 5**. It is observed that the S1223 and MA409 airfoils have the highest aerodynamic efficiency among the investigated airfoils where the S1223 is found to be performing more efficiency than MA 409 by 8% only while the lift coefficient of S1223 is 54% higher than MA409 and this explains the significantly low drag coefficient of MA409. However , despite the higher drag of S1223 airfoil , it is identified to be the more aerodynamically efficient candidate for the new wing design having considered the importance of zero angle of attack lift coefficient which is mandatory for cruising phase of the small UAVs.
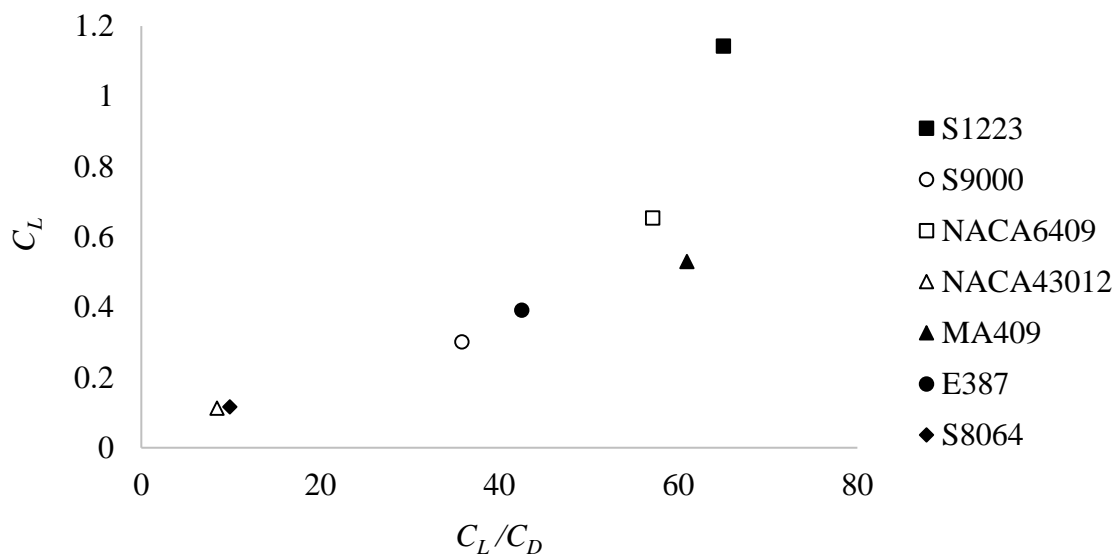

Figure 5. Aerodynamic efficiency and C_{L0} of different low speed aifoils.

3.3. Aspect Ratio and Sweep Compromise

Aerodynamic efficiency optimization of a wing is built upon a compromise of wing design parameters such as aspect ratio, tapper ratio and quarter chord sweep angle. The results obtained from numerical simulations (**Figure 6**) are discussed in this section and the effect of wing parameters changes on aerodynamic efficiency behavior of different wings with equal frontal area are evaluated. It is observed that the C_D of Wing 4 and Wing 5 with aspect ratio of 1.8 is less than the C_D of the Wing 1, Wing 2 and Wing 3 with aspect ratio of 1. The drag force of a three-dimensional wing at low speeds is significantly affected by an additional drag component called induced drag (C_{Di}) that is generated due to wing tip vortex. The induced drag is inversely proportional to aspect ratio. Hence; as the aspect ratio is increased, lower amount of flow is interchanged between the upper (low pressure zone) and lower (high pressure zone) surfaces of the wing since the span of the wing is increased and tip chord is decreased. Consequently, lower wing tip vortices are generated and the induced drag is reduced and as a result, the total drag of the wing is reduced which is desired to optimize the wing aerodynamic efficiency and enhance the flight endurance. Mueller and De Laurier experimental findings on low aspect ratio wings show the similar induced drag behavior (Mueller and De Laurier, 2003). The analysis of lift coefficients for different wings is illustrated in **Figure 6** shows 16.7% increase in the amount of lift generated by wing with quarter chord sweep of 16° as the aspect ratio is increased from 1 (Wing 2) to 1.8 (Wing 4) while comparison of the wings with no quarter chord sweep demonstrates 31% reduction in the generated lift as the aspect ratio is increased from 1 (Wing 3) to 1.8 (Wing 5). Also, comparison of the aerodynamic efficiency of the investigated wings (**Figure 7**) shows that Wing 4 with aerodynamic efficiency of 7.15 has the highest aerodynamic efficiency and lift coefficient among the five wing planforms which explains the compromise of the increased aspect ratio and swept wing.
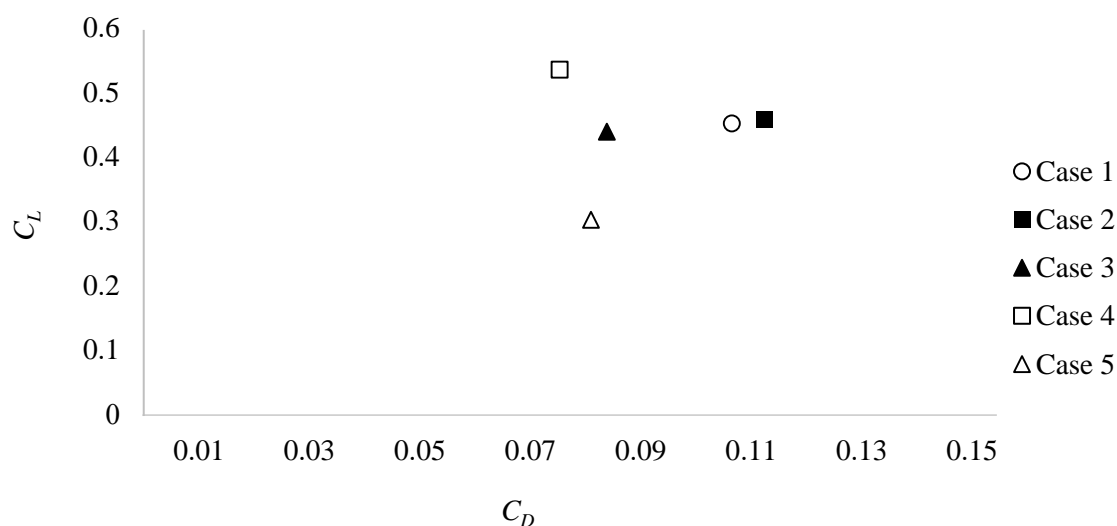

Figure 6. Drag polar for different wings.

The pressure distribution on the wing geometries is emphasized in **Figure 8**. Comparison of the pressure contours demonstrates that the amount of pressure on the upper surface of the wing close to wing tip is reduced for the wings with higher aspect ratio (Wing 4 and 5). This again is a result of lower wing tip vortices effect on wings with higher aspect ratio. However, the pressure on the upper surface of Wing 5 is observed to be increased towards the root chord of the wing which caused the wing to have lower lift coefficient compared to other wings. The observations obtained from the comparison of the different wings and compromise of the aspect ratio and sweep angle are utilized in the design of the new wing geometry with optimized aerodynamic efficiency and enhanced flight endurance.

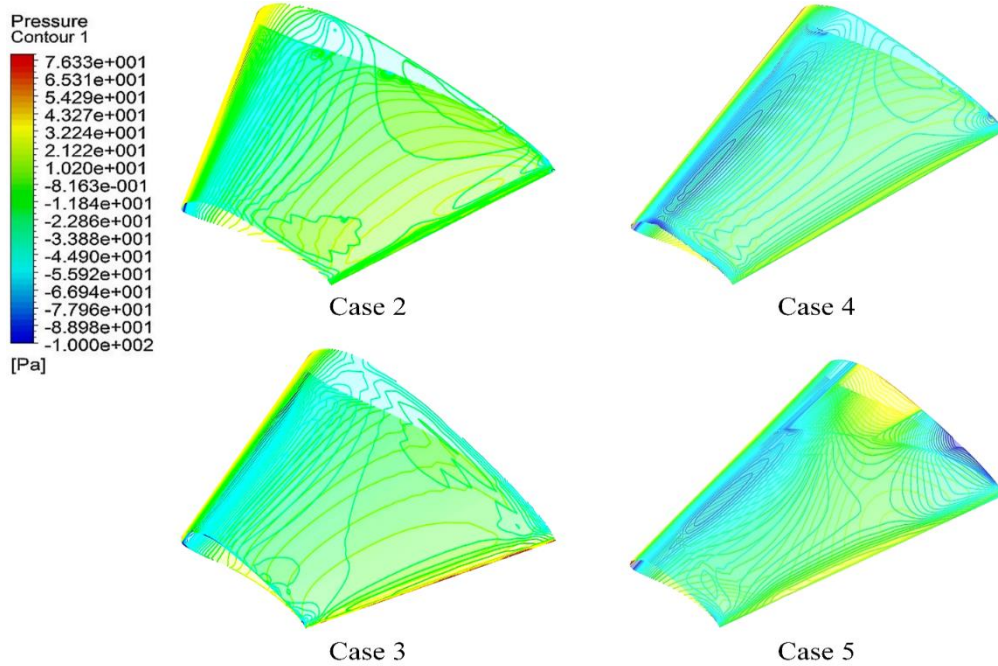**Figure 7.** Aerodynamic efficiency comparison of the wings.

Figure 8. Pressure distribution over the wings.

3.4. Optimized Wing Planform Aerodynamic Performance

The main purpose of wing performance optimization is to increase the endurance of a flying MUAV. Literature findings is evident of alpine swift wing excessive endurance with 200 days of non-stop flight (Liechti *et al.,* 2013). A combination of the biomimicry of alpine swift bird's wing and results obtained from airfoil selection as well as aspect ratio and sweep compromise phases lead to a new wing planform named as Alpine wing. As it is observed in previous sections, a wing with S1223 airfoil section and a compromise of increased aspect ratio and sweep angle can be utilized to achieve a wing planform with optimum performance. Also, the previous studies suggest that applying raked wingtip plays an important role in reduction of wing tail vortex and induced drag. Hence, a raked wing tip extension is also applied to the tip panel of the designed Alpine wing planform. The aerodynamic performance of Alpine wing is evaluated through numerical simulations (**Figures 9** and **10**). The new wing aerodynamic efficiency and corresponding lift coefficient is compared with the wing designs in previous section and an existing reference wing in literature (DeLuca *et al.,* 2006). Comparisons show that the Alpine wing is observed to have lift coefficient and aerodynamic efficiency of 0.675 and 8.715, respectively. The observations demonstrate 25.5% improvement of lift coefficient for Alpine wing compared to Wing 4 while the aerodynamic efficiency of Alpine wing is observed to be increased by 21% compared to Wing 4 which means that the Alpine wing drag coefficient is 4% higher than Wing 4. The small increment in the drag coefficient is caused by the forward quarter chord sweep of the root panel and interference drag due to interference of the three swept panels of Alpine wing. But, the enhanced aerodynamic efficiency of Alpine wing confirms that the achieved lift coefficient improvement compensates for the slight increase in the drag coefficient and an optimized wing geometry is achieved.
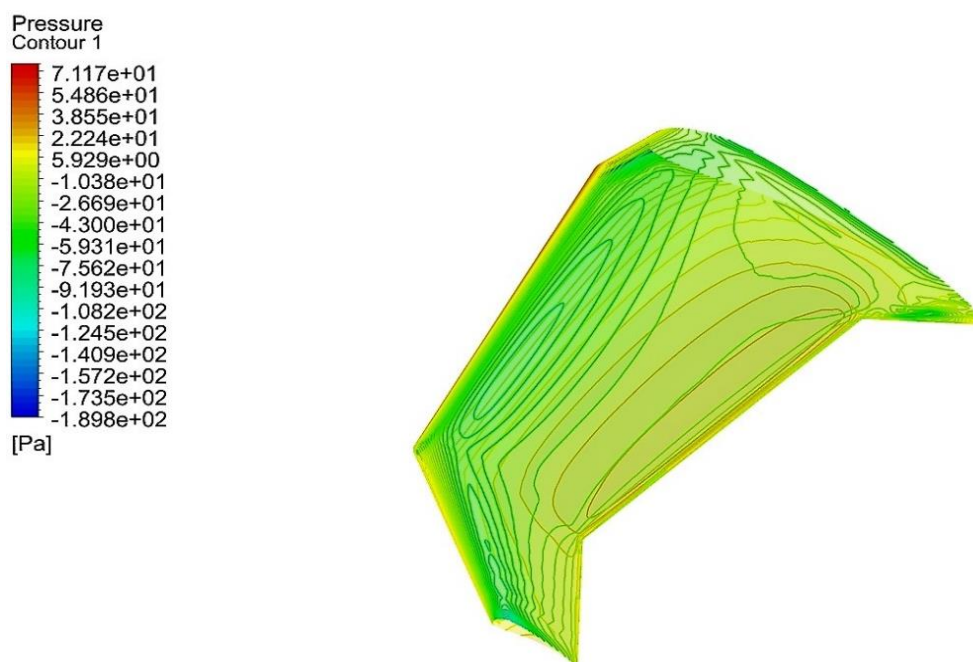

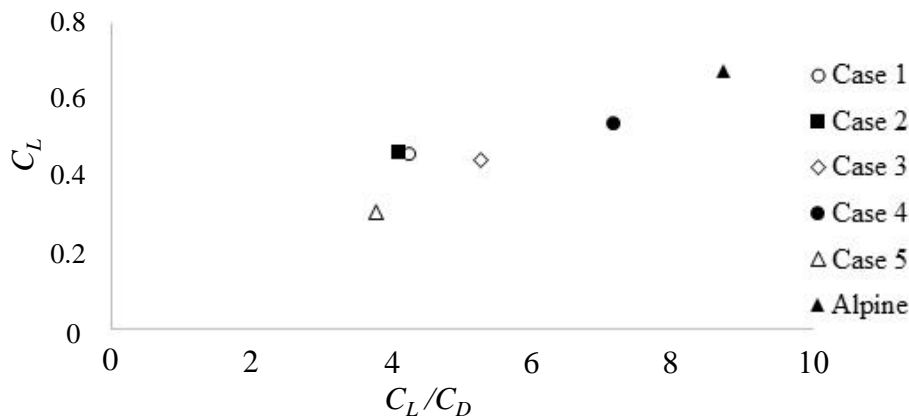**Figure 9.** Pressure distribution on the alpine wing.

Figure 10. Numerical evaluation of alpine wing aerodynamic performance.

One final assessment of the Alpine performance optimization is conducted by comparison of its aerodynamic efficiency with an existing reference wing with similar boundary conditions that was studied by Deluca *et al.* (2006). The reference wing has an elliptical planform with area of $0.03\,\mathrm{m}^2$ and an aerodynamic efficiency of 7.76. Comparison of the numerically calculated characteristics of Alpine wing with experimental results of the reference wing shows that the lift coefficient and aerodynamic efficiency of the Alpine wing are improved by 14.4 and 12.26%, respectively, which again is an affirmation of the optimization of the Alpine wing performance.

3.5. Validation of Wings Numerical Simulation Results

The validity of the obtained numerical results is assessed by wind tunnel experiments conducted on Wing 1 (average aerodynamic efficiency), Wing 4 (high aerodynamic efficiency), Wing 5 (low aerodynamic efficiency) and Alpine (optimum aerodynamic efficiency). As it is illustrated in **Figure 11**, comparison of the lift coefficients obtained from numerical simulations with wind tunnel experiments shows inaccuracies ranging from 8 to 18% which correspond to Alpine and Wing 4 planforms, respectively. Moreover, it is observed that the numerically calculated drag coefficient differs from wind tunnel experiments with a minimum of 2.5% and maximum of 14.5% for Wing 4 and Alpine respectively. The minor deviation of the numerical results from wind tunnel experiments suggest that a more refined mesh with smaller element size near the wing geometry can be utilized to achieve more accurate results. However, the trend of the numerical and experiments results complement each other. Therefore, no additional time and computational cost is required to be spent on numerical simulation by refining the mesh since the objective of this research is not to increase the accuracy of numerical results but to achieve optimized wing geometry. Analysis of the Alpine wing numerical and experimental results validation shows that the Alpine 's experimental aerodynamic efficiency has a value of 10.870 that is 19.8% higher than the numerically calculated aerodynamic efficiency and 35.9% higher than the existing reference wing.
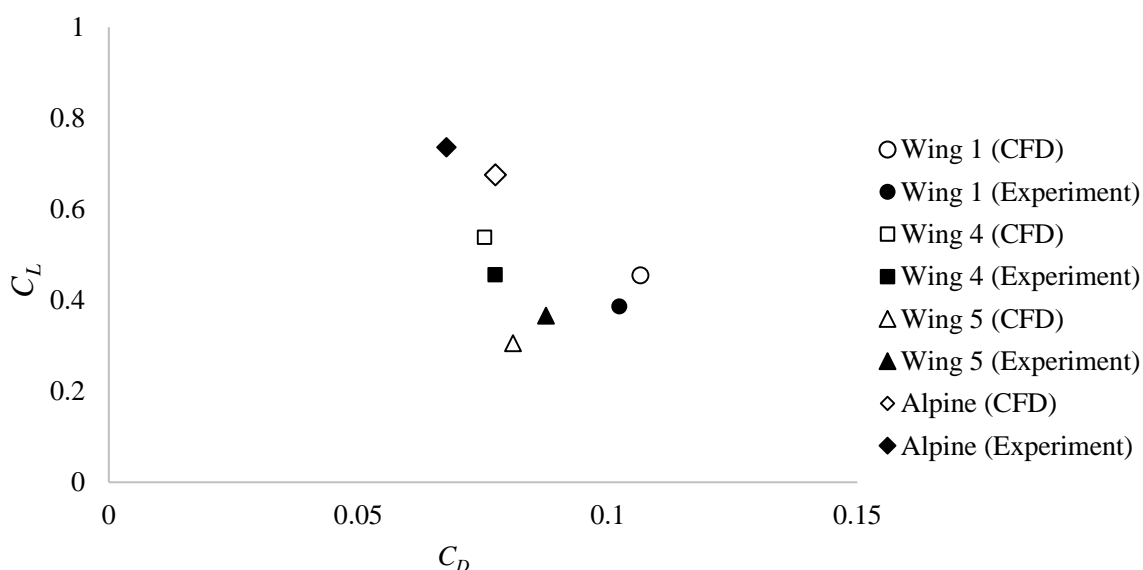
Figure 11. Validation of drag polar for different wings.

4. CONCLUSION

In the present research, the aerodynamic performance enhancement of a cruising fixed wing MUAV is studied by evaluation of the effects of wing shape and the design parameters on the aerodynamic efficiency and achieve a compromise of aspect ratio and quarter chord sweep. A new wing geometry is designed and named as Alpine since it is inspired by biomimicry of alpine swift bird. The comparison of the Alpine wing planform with existing reference wing geometry at similar operating conditions and same wing area shows that the Alpine wing aerodynamic performance is more efficient compared to the reference elliptical wing by 35.9% which confirms the achievement of a wing design with optimized aerodynamic performance. Hence; utilizing the Alpine wing planform equips a cruising MUAV with optimized aerodynamic efficiency and enhanced endurance.

5. ACKNOWLEDGEMENTS

5. AUTHORS' NOTE

The author(s) declare(s) that there is no conflict of interest regarding the publication of this article. Authors confirmed that the data and the paper are free of plagiarism.

6. REFERENCES

Abdulrahim, M., Watkins, S., Segal, R., Marino, M., and Sheridan, J. (2010). Dynamic sensitivity to atmospheric turbulence of unmanned air vehicles with varying configuration. *Journal of Aircraft*, *47*(6), 1873-1883.

Ananda, G. K., Sukumar, P. P., and Selig, M. S. (2015). Measured aerodynamic characteristics of wings at low Reynolds numbers. *Aerospace Science and Technology*, *42*, 392-406.

Bronz, M., Hattenberger, G., and Moschetta, J. M. (2013). Development of a long endurance mini-uav: Eternity. *International Journal of Micro Air Vehicles*, *5*(4), 261-272.

Chahl, J. (2015). Unmanned aerial systems (UAS) research opportunities. *Aerospace*, *2*(2), 189-202.

DeLuca, A. M., Reeder, M. F., Freeman, J. A., and Ol, M. V. (2006). Flexible-and rigid-wing micro air vehicle: lift and drag comparison. *Journal of Aircraft*, *43*(2), 572-575.

Drovetski, S. V. (1996). Influence of the trailing-edge notch on flight performance of galliforms. *The Auk*, *113*(4), 802-810.

Eftekhri , S., and Al-Obaidi , A. S. M. (2019). Investigation of a NACA 0012 Finite Wing Aerodynamics at Low Reynold's Numbers and 0 ° to 90 ° Angle of Attack . *Journal of Aerospace Technology and Management*, *11*, e1519.

Ghazzai, H., Ghorbel, M. B., Kadri, A., Hossain, M. J., and Menouar, H. (2017). Energy-efficient management of unmanned aerial vehicles for underlay cognitive radio systems. *IEEE Transactions on Green Communications and Networking*, *1*(4), 434-443.

Giguere, P., and Selig, M. S. (1998). New airfoils for small horizontal axis wind turbines. *Journal of Solar Energy Engineering*, *120*(2), 108-114.

Hain, R., Kähler, C. J., and Radespiel, R. (2009). Dynamics of laminar separation bubbles at low-Reynolds-number aerofoils. *Journal of Fluid Mechanics*, *630*, 129-153.

Kim, D. H., and Chang, J. W. (2014). Low-Reynolds-number effect on the aerodynamic characteristics of a pitching NACA0012 airfoil. *Aerospace Science and Technology*, *32*(1), 162-168.

Kontogiannis, S. G., and Ekaterinaris, J. A. (2013). Design, performance evaluation and optimization of a UAV. *Aerospace Science and Technology*, *29*(1), 339-350.

Kumar, R. S., Sivakumar, V., Ramakrishnananda, B., Arjhun, A.K., and Suriyapandiyan (2017). Numerical investigation of two element camber morphing airfoil in low reynolds number flows. *Journal of Engineering Science and Technology*, *12*(7), 1939-1955.

Lei, Z. (2005). Effect of RANS turbulence models on computation of vortical flow over wing-body configuration. *Transactions of the Japan Society for Aeronautical and Space Sciences*, *48*(161), 152-160.

Liechti, F., Witvliet, W., Weber, R., and Bächler, E. (2013). First evidence of a 200-day non-stop flight in a bird. *Nature Communications*, *4*, 2554.

Martínez-Aranda, S., García-González, A. L., Parras, L., Velázquez-Navarro, J. F., and Del Pino, C. (2016). Comparison of the aerodynamic characteristics of the NACA0012 airfoil at low-to-moderate Reynolds numbers for any aspect ratio. *International Journal of Aerospace Sciences*, 4(1), 1-8.

Mueller, T. J., and DeLaurier, J. D. (2003). Aerodynamics of small vehicles. Annual Review of Fluid Mechanics, 35(1), 89-111.

Panagiotou, P., Kaparos, P., and Yakinthos, K. (2014). Winglet design and optimization for a MALE UAV using CFD. Aerospace Science and Technology, 39, 190-205.

Sathaye, S., Yuan, J., and Olinger, D. (2004). Lift Distributions on Low-Aspect-Ratio Wings at Low Reynolds Numbers for Micro -Air Vehicle Applications . In 22 nd Applied Aerodynamics Conference and Exhibit (p. 4970).

Shah, H., Mathew, S., and Lim, C. M. (2015). Numerical simulation of flow over an airfoil for small wind turbines using the gamma-theta model. *International Journal of Energy and Environmental Engineering*, *6*(4), 419-429.

Shukla, A., and Karki, H. (2016). Application of robotics in onshore oil and gas industry—A review Part I. *Robotics and Autonomous Systems*, *75*, 490-507.